AJNR Am J Neuroradiol 19:253–259, February 1998

Three-dimensional FISP Imaging in the Evaluation of Carotid Cavernous Fistula: Comparison with Contrast-Enhanced CT and Spin-Echo MR

Toshinori Hirai, Yukunori Korogi, Satoshi Hamatake, Ichiro Ikushima, Takeshi Sugahara, Yoshinori Sigematsu, Yoshiharu Higashida, and Mutsumasa Takahashi

PURPOSE: **The purpose of this study was to assess the value of three-dimensional fast imaging with steady-state precession (FISP) MR sequences relative to contrast-enhanced CT and spin-echo MR imaging in the diagnosis of carotid cavernous fistula (CCF).**

METHODS: **Seventeen patients with 19 angiographically proved CCFs had contrast-enhanced CT, spin-echo MR imaging, and 3-D FISP imaging. Three observers assessed these imaging studies as well as those of 43 control sides in a blinded manner for the presence or absence of CCF. Receiver operating characteristic analysis was used to assess the diagnostic utility of each imaging technique. In a nonblinded study, contrast-enhanced 3-D FISP images were also evaluated.**

RESULTS: **Higher diagnostic accuracy was obtained with 3-D FISP sequences, as the shunt flow within the cavernous sinus was well seen. Sensitivity of 3-D FISP images was 83% and specificity was 100% in the blinded study. In the receiver operating characteristic analysis, the diagnostic performance of observers was found to be better with the 3-D FISP images than with the spin-echo MR images. Although there were no significant difference between 3-D FISP and contrast-enhanced CT, higher diagnostic performance was obtained with 3-D FISP images. In three CCFs without anterior drainage, a diagnosis was made only from the 3-D FISP images. The contrast-enhanced 3-D FISP images were not helpful, since the cavernous sinuses enhanced.**

CONCLUSION: **Three-dimensional FISP imaging is superior to spin-echo MR imaging and contrast-enhanced CT in the diagnosis of CCF. Contrast-enhanced 3-D FISP images are not helpful for the evaluation of CCF.**

The diagnosis of carotid cavernous fistula (CCF) depends primarily on findings at catheter angiography. Previous reports have shown that contrast-enhanced computed tomography (CT) and spin-echo magnetic resonance (MR) imaging are helpful in the assessment of CCFs (1–5). On CT scans, the diagnosis depends on morphologic changes, such as enlargement of the superior ophthalmic veins, cavernous sinus, and/or extraocular muscles, and protrusion of the globe. Spin-echo MR imaging is able to depict flow voids in the involved cavernous sinus. Recently, the clinical efficacy of using the source images of three-dimensional Fourier transform time-of-flight MR angiography has been reported (6–8). The source images from MR angiography contain both flow and anatomic information. Small intracranial structures, such as cranial nerves, can be seen by virtue of the high resolution provided by acquisition of submillimeter sections and flow-related enhancement. Although the maximum intensity projection algorithm provides angiogramlike images, the lower signal intensity features of the vessels may be lost, resulting in a loss of visibility of small or slow-flowing vessels (9). Therefore, we used only the source images of MR angiography in our evaluation of CCFs.

Flow-related enhancement of the cavernous sinus has been reported in a patient with CCF (10). The purpose of this study was to evaluate the diagnostic accuracy of the axial source images from 3-D time-of-flight MR angiography as compared with contrast-enhanced CT scans and spin-echo MR images.

Received May 12, 1997; accepted after revision August 19.

From the Department of Radiology, Kumamoto University School of Medicine, 1–1–1 Honjo Kumamoto 860, Japan. Address reprint requests to Toshinori Hirai, MD.

Methods

Patients and Control Subjects

Seventeen consecutive patients (five men and 12 women; age range, 18 to 76 years; mean age, 56 years) with angiographically proved CCFs underwent examination with contrast-enhanced CT, spin-echo MR imaging, and 3-D MR imaging. The imaging examinations, including contrast angiography, were performed within 14 days of one another. Dural CCFs were present in 14 patients; three patients had direct CCFs. Clinical signs and symptoms included diplopia, headache, bruit, exophthalmos, chemosis, cranial nerve palsy, and decline of visual acuity.

Contrast angiography was performed by using a digital subtraction technique with bilateral selective catheterization of the external and internal carotid arteries. Bilateral CCFs were seen in two patients. Thus, a total of 19 CCFs in 17 patients were included in this study. The drainage vessels included 15 superior ophthalmic veins (SOVs), three inferior ophthalmic veins, 11 inferior petrosal sinuses, two superior petrosal sinuses, and five cortical veins. Anterior drainage was not seen in three of 17 patients; drainage was into the inferior petrosal sinus in two of these patients and into the cortical veins in the other. Drainage into the contralateral cavernous sinus through the intercavernous sinus was seen in six of 15 patients with unilateral CCFs.

On the basis of the drainage flow speed, we classified CCFs into three types: when the main drainage was seen entirely during the early arterial phase, the CCF was defined as a fast type (n = 10); when the main drainage was seen entirely during the midarterial phase, the CCF was defined as a moderate type (n = 4); and when the main drainage was seen entirely during the late arterial to venous phase, the CCF was defined as a slow type (n = 5).

The control group consisted of 17 age-matched patients (seven men and eight women; age range, 17 to 76 years; mean age, 55 years) whose studies were selected from a consecutive series of routine contrast-enhanced CT examinations. Criteria for inclusion in this group were no clinical evidence of a CCF, CT scans with a section thickness of 5 mm or less in the axial plane with no intersection gap, use of contrast material, and no CT evidence of a mass lesion from the orbit to the cavernous sinus. Indications for CT in these cases included posttreatment evaluation of orbital pseudotumor (n = 6), visual disturbance (n = 5), posttreatment evaluation of malignant lymphoma (n = 2), swelling of the eyelid (n = 2), glaucoma (n = 1), and hyperthyroidism with ophthalmopathy (n = 1). As the control group for spin-echo MR imaging, the studies of 17 age-matched patients (three men and 14 women; age range, 14 to 72 years; mean age, 54 years) were also selected from a consecutive series of routine MR examinations. Criteria for inclusion in this group were no clinical evidence of CCF, section thickness of 5 to 6 mm in the coronal and/or axial plane on spin-echo images, and no mass lesion from the orbit to the cavernous sinus on spin-echo images. Indications for spin-echo MR imaging included posttreatment evaluation of orbital pseudotumor (n = 7), optic nerve atrophy (n = 3), optic neuritis (n = 2), hyperthyroidism (n = 2), visual disturbance (n = 2), and swelling of the eyelid (n = 1). The control group for 3-D MR imaging included the imaging examinations of 12 healthy volunteers (10 men and two women; age range, 26 to 58 years; mean age, 32 years) and four patients with trigeminal neuralgia (four women; age range, 40 to 66 years; mean age, 56 years). The trigeminal neuralgia studies were selected from a series of MR examinations in which the cavernous sinus was located at the center of the volume slab. A saturation pulse was not used in this control group.

Images of nine sides in 15 patients with unilateral CCF were also included as control studies. We excluded six contralateral sides in six patients with CCF from the blinded study in whom drainage was through the intercavernous sinus, because angiograms did not actually depict a CCF on this side. Thus, 62 sides (19 in patients with CCF and 43 control studies) were evaluated in the blinded study of CT and spin-echo MR imaging. Three-dimensional MR images were not obtained in one patient with CCF whose drainage was through the intercavernous sinus; therefore, 59 sides (18 in patients with CCF and 41 control studies) were evaluated in the blinded study of 3-D MR imaging.

Imaging Methods

All CT examinations were performed with a commercially available CT scanner. All CT scans were obtained through the orbit and parasellar regions after intravenous infusion of 100 mL of iodinated contrast medium. The scans were obtained in the axial plane with thicknesses of 1.5 mm (n = 5), 3 mm (n = 9), and 5 mm (n = 3) with no intersection gap.

MR examinations were performed with two different models of 1.5-T superconductive units. First, routine T1-weighted (600/15/1 [repetition time/echo time/excitations]) and T2-weighted (2300/90/1) spin-echo images were obtained in the axial and/or coronal plane through the orbit and parasellar regions. All images were obtained with a 22-cm field of view and a 192 × 256 matrix. Section thickness was 5 to 6 mm with a 1.0 to 1.2 mm intersection gap.

Three-dimensional fast MR imaging with steady-state precession (FISP) was performed with the following parameters: 20/6–7/1, 15 to 20° flip angle, 50- to 64-mm slab thickness, 50 to 64 partitions, 22-cm field of view, and 192–256 × 256–512 matrix. The actual thickness of the partitions was 0.8 to 1.0 mm. Velocity compensation was applied in the read and section-select directions. The saturation pulse was not used above the volume slab in any patient except one, who was imaged with a Magnetom Vision unit. The cavernous sinus was located at the center of the volume slab, which was oriented axially and included draining vessels from the cavernous sinus. The 3-D FISP images were also obtained after intravenous administration of gadopentetate dimeglumine in 11 of 17 patients with CCF.

Interpretation of Images

Contrast-enhanced CT scans, spin-echo MR images, and 3-D FISP images were reviewed in a blinded, random manner by three observers. When imaging studies from one technique were being analyzed, information from the other technique or from contrast catheter angiography or from clinical records was not available to the reviewers. For each of the three imaging techniques, the readers recorded the presence or absence of CCF as well as any abnormality identified in the cavernous sinus and superior ophthalmic vein.

In keeping with previous reports (1, 5), a CT diagnosis of CCF was made if focal bulging or diffuse distention of the cavernous sinus, enlargement of the superior ophthalmic vein, or both were present. Ancillary findings, such as proptosis or enlargement of the extraocular muscles, were excluded from this study. For spin-echo MR imaging, the presence of a flow void within the cavernous sinus was added. The criteria for a diagnosis of CCF on 3-D FISP images included the presence of hyperintense regions within the cavernous sinus in addition to the other criteria.

After the blinded study, the cavernous sinus and drainage pathways (superior ophthalmic vein, superior and inferior petrosal sinus, cortical vein) were reviewed retrospectively by two radiologists in consensus, together with the clinical and angiographic findings. The 3-D FISP images obtained after the injection of contrast material were also evaluated to determine whether contrast enhancement improved the ability to diagnose CCF.

Analysis of Data

The receiver operating characteristic (ROC) analysis was used to assess the ability to establish the presence or absence of CCF with each technique (11, 12). Observers were asked to

state their judgment with regard to the presence or absence of CCF by means of a five-point rating scale (1 = definitely absent, 2 = probably absent, 3 = possibly present, 4 = probably present, 5 = definitely present). To evaluate overall detection, average ROC curves were calculated from individual ROC data by means of the program by Metz (13, 14). Diagnostic accuracy was determined from the area under the ROC curve (A_z). A_z values were used to analyze the statistical significance of the differences in observer performance by means of the paired Student's *t* test.

Answers of "definitely present" and "probably present" were considered positive for the prediction of CCF. Sensitivity, specificity, and accuracy in the detection of CCF were calculated for each imaging technique.

Results

Three-dimensional FISP images showed isointense signal relative to brain tissue within the cavernous sinus on all 41 control sides (Fig 1). Hyperintense areas within the cavernous sinus were not observed.

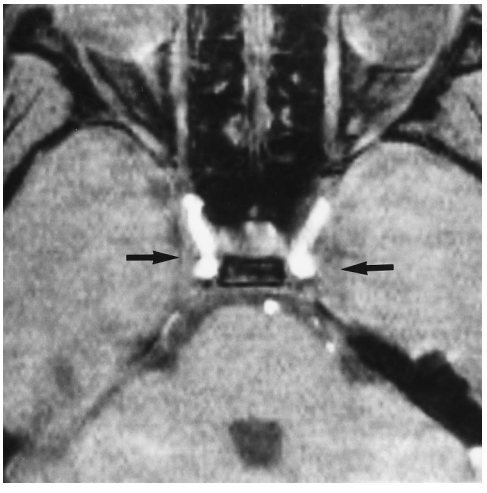

FIG 1. Three-dimensional FISP image in a healthy volunteer shows that the cavernous sinuses (*arrows*) are isointense with brain.

Table 1 presents a summary of the confidence ratings for each observer. Average ROC curves for the determination of presence or absence of CCF with contrast-enhanced CT, spin-echo MR imaging, and 3-D FISP imaging are compared in Figure 2. Diagnostic accuracy was highest with 3-D FISP imaging and lowest with spin-echo MR imaging. Table 2 summarizes the A_z values, sensitivities, and accuracies for all three techniques for individual observers. In ROC analysis, the diagnostic performance of observers was found to be better with 3-D FISP imaging than with spin-echo MR imaging ($P = .01$). Although there were no significant differences between 3-D FISP images and contrast-enhanced CT scans, higher diagnostic performance was obtained with 3-D FISP images. The diagnostic performance of observers was better with contrast-enhanced CT than with spin-echo MR imaging ($P = .05$). The sensitivities of contrast-enhanced CT, spin-echo MR imaging, and 3-D FISP imaging were 72%, 56%, and 83%, respectively, with specificities of 97%, 93%, and 100%, respectively. The accuracies of contrast-enhanced CT, spin-echo MR imaging, and 3-D FISP imaging were 89%, 82%, and 95%, respectively.

In the blinded study, the cavernous sinus involved by a CCF was identified correctly on 29 (51%) of 57 contrast-enhanced CT scans, on 19 (33%) of 57 spin-echo MR images, and on 43 (80%) of 54 3-D FISP images (19, 19, and 18 cavernous sinuses, respectively, × three observers) (Fig 3). Ten (8%) and four (3%) of 129 observations (43 cavernous sinuses × three observers) were misinterpreted as dilatation or flow void on contrast-enhanced CT scans and spin-echo images, respectively. There were no false-positive findings with 3-D FISP images. All three CCFs in

TABLE 1: Confidence ratings of observers in the diagnosis of carotid cavernous fistula (CCF)

	CCF Side (n = 19)			Control Side (n = 43)		
	Observer			Observer		
	A	B	C	A	B	C
Contrast-enhanced CT						
Definitely absent	1	0	0	26	16	3
Probably absent	2	2	2	10	17	30
Possibly present	4	3	2	7	7	9
Probably present	4	4	11	0	3	1
Definitely present	8	10	4	0	0	0
Spin-echo MR imaging						
Definitely absent	3	2	0	25	16	4
Probably absent	1	4	7	12	20	27
Possibly present	3	2	3	5	3	8
Probably present	4	3	6	1	4	4
Definitely present	8	8	3	0	0	0
3-D FISP MR imaging*						
Definitely absent	0	1	0	26	29	9
Probably absent	2	1	3	12	10	29
Possibly present	0	1	1	3	2	3
Probably present	5	2	8	0	0	0
Definitely present	11	13	6	0	0	0

* For this technique, there were 18 CCF sides and 41 control sides.

which the anterior drainage was not observed were judged as negative on contrast-enhanced CT and spin-echo MR studies, whereas they were diagnosed correctly on the 3-D FISP images (Fig 3). The SOV drainage was identified correctly in 36 (80%) of 45, 24 (53%) of 45, and 28 (67%) of 42 observations (15, 15, and 14 CCFs × three observers), respectively. For the control sides, six (4%) of 141, four (3%) of 141, and two (1%) of 138 observations (47, 47, and 46 SOVs × three observers) were evaluated as dilatation on contrast-enhanced CT scans, spin-echo MR images and 3-D FISP images, respectively.

In the retrospective study, the cavernous sinus involved by a CCF was identified correctly on contrast-enhanced CT scans and spin-echo images in 11 (58%) and nine (47%) of 19 CCFs, respectively. Hyperintense areas within a cavernous sinus were interpreted correctly on 3-D FISP images in 15 (83%) of 18 CCFs (Fig 3B). All CCFs showing hyperintensity within the cavernous sinus on 3-D FISP images were the fast- to moderate-type CCF, whereas three CCFs that did not show hyperintensity in the cavernous sinuses were the slow type. Multiple hyperintense curvilinear structures or spots adjacent to or within a cavernous sinus were also observed in five of seven fast-type dural CCFs (Fig 3B). However, this finding was not seen in direct CCFs. SOV drainage was interpreted correctly on contrast-enhanced CT scans, spin-echo MR images, and 3-D FISP images in 13 (87%) of 15, 10 (67%) of 15, and 12 (86%) of 14 SOVs, respectively. Hyperintensity of SOV drainage was seen in seven of 14 cases on 3-D FISP images.

On contrast-enhanced CT scans, inferior petrosal sinus drainage was identified correctly in three of 11 cases. On spin-echo axial MR images, the flow void of the inferior petrosal sinus was identified in three of six cases, whereas all eight inferior petrosal sinus drainage vessels were identified as hyperintense structures on 3-D FISP images (Fig 3C). Two drainages to the superior petrosal sinus were not seen on either CT or spin-echo MR studies, whereas they were correctly identified on the 3-D FISP images. Cortical venous drainage was identified correctly on CT, spin-echo MR, and 3-D FISP studies in three, two, and two of five cases, respectively.

On the contrast-enhanced studies, bilateral cavernous sinuses enhanced homogeneously in 10 of 11 cases. In a patient with a direct CCF, the contralateral cavernous sinus did not enhance homogeneously, probably because of thrombosis. Drainage vessels enhanced homogeneously in all cases. Contrast-enhanced studies provided no additional information to that obtained from the noncontrast 3-D FISP images.

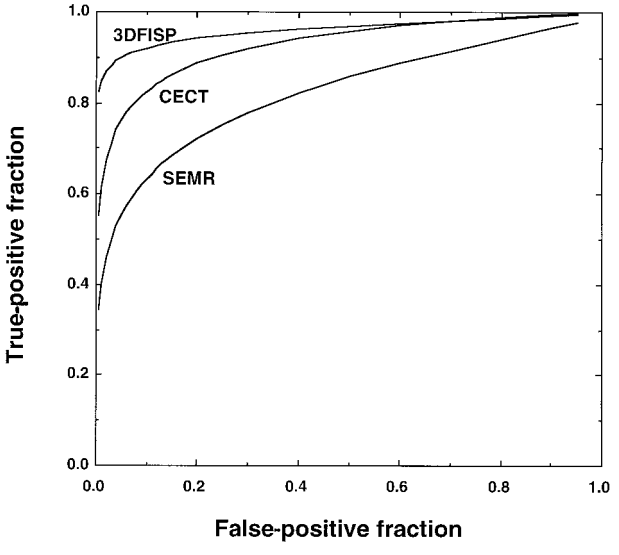

FIG 2. ROC analysis compares the confidence of observers in establishing the presence or absence of CCF with contrast-enhanced CT (*CECT*), spin-echo MR imaging (*SEMR*), and 3-D FISP imaging (*3DFISP*).

Discussion

For all control sides, 3-D FISP images showed isointense signal relative to brain tissue within the cavernous sinuses. Because blood-flow velocity in a normal cavernous sinus is slow, the blood flow within the structure is saturated and does not show flow-related enhancement. Therefore, hyperintense areas within a cavernous sinus in patients with CCF may be considered abnormal.

In the blinded study, the highest diagnostic accuracy was obtained with 3-D FISP imaging. This result is attributed to the high detectability of the abnormal cavernous sinus. Presence of hyperintense areas within the cavernous sinus on 3-D FISP images was a more reliable finding than was enlargement of the cavernous sinus on contrast-enhanced CT or spin-echo MR studies. In the ROC analysis, the diagnostic performance of the observers was significantly better on the 3-D FISP images than on the spin-echo MR images. Although there was no significant difference between 3-D FISP images and contrast-enhanced CT

TABLE 2: A_z, sensitivity, specificity, and accuracy values for each observer by imaging technique

Observer	A_z			Sensitivity			Specificity			Accuracy		
	Contrast-Enhanced CT	Spin-Echo MR	3-D FISP	Contrast-Enhanced CT	Spin-Echo MR	3-D FISP	Contrast-Enhanced CT	Spin-Echo MR	3-D FISP	Contrast-Enhanced CT	Spin-Echo MR	3-D FISP
A	0.93	0.85	0.98	0.63	0.63	0.89	1.00	0.98	1.00	0.89	0.87	0.97
B	0.93	0.82	0.95	0.74	0.58	0.83	0.93	0.91	1.00	0.87	0.81	0.95
C	0.94	0.78	0.95	0.79	0.47	0.78	0.98	0.91	1.00	0.92	0.77	0.93
Overall	0.93	0.82	0.96	0.72	0.56	0.83	0.97	0.93	1.00	0.89	0.82	0.95

Note.—3-D FISP indicates three-dimensional FISP MR imaging. Overall values are expressed as the mean.

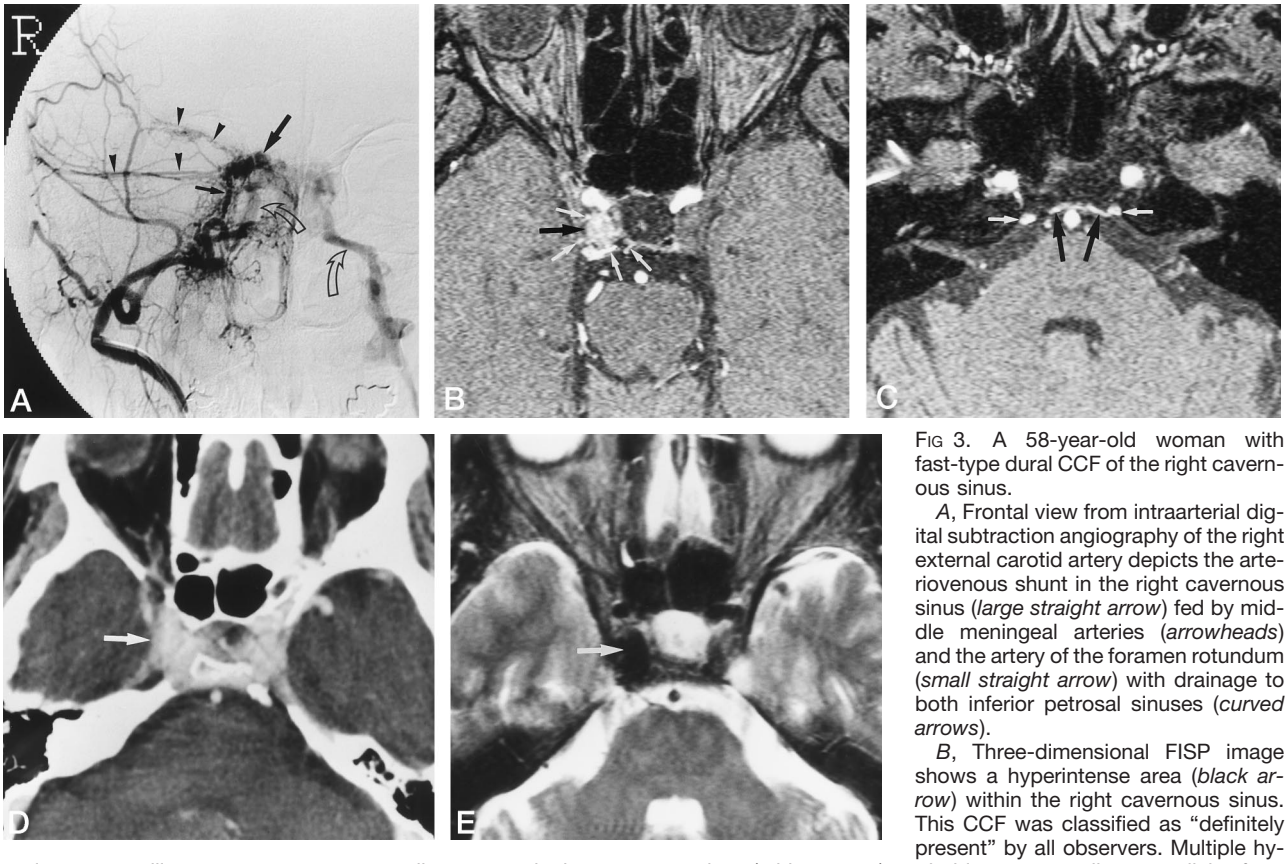

FIG 3. A 58-year-old woman with fast-type dural CCF of the right cavernous sinus.

A, Frontal view from intraarterial digital subtraction angiography of the right external carotid artery depicts the arteriovenous shunt in the right cavernous sinus (*large straight arrow*) fed by middle meningeal arteries (*arrowheads*) and the artery of the foramen rotundum (*small straight arrow*) with drainage to both inferior petrosal sinuses (*curved arrows*).

B, Three-dimensional FISP image shows a hyperintense area (*black arrow*) within the right cavernous sinus. This CCF was classified as "definitely present" by all observers. Multiple hyperintense curvilinear structures or spots adjacent to or in the cavernous sinus (*white arrows*), probably corresponding to pedicles from the meningohypophyseal or middle meningeal arteries, are also seen.

C, Three-dimensional FISP image caudal to *B* shows hyperintensity in the inferior petrosal sinus bilaterally (*white arrows*) and in the clival venous plexus (*black arrows*).

D, Contrast-enhanced CT scan shows no definite bulging of the lateral wall of the slightly enlarged right cavernous sinus (*arrow*). Two observers classified it as "probably absent," whereas one observer classified it as "possibly present."

E, Axial T2-weighted MR image shows a hypointense area within the right cavernous sinus (*arrow*). This abnormal flow void may be difficult to differentiate from the flow void of an enlarged internal carotid artery.

scans, higher diagnostic performance was obtained with the 3-D FISP images. Our sample size and the number of observers were small, and a study with a larger sample size and more observers may yield significant differences.

In three CCFs without anterior drainage, a diagnosis was made only with the 3-D FISP images. This indicates that contrast-enhanced CT scans and spin-echo MR images are limited in their ability to depict an abnormal cavernous sinus. Some authors have reported the detection of a focal bulging or diffuse distention of a cavernous sinus on thin-section contrast-enhanced CT scans in 50% to 64% of patients with CCF (1, 5). In our study, the detectability of this abnormal finding on contrast-enhanced CT scans was nearly equal to that of previous reports. Since the abnormal contour of the lateral wall of the cavernous sinus is an indirect sign, its detection rate with CT may be relatively low. A flow void within the cavernous sinus on spin-echo MR images in patients with CCF has been described (2, 3, 5). In our study, a flow void within the involved cavernous sinus was not identified frequently on spin-echo MR images. Most patients in our study had dural CCFs. The difference in the selection of patients may have resulted in a lower detection rate. In our blinded study, four (3%) of 129 observations were misinterpreted as flow void on spin-echo MR images. In these false-positive cases, hypointense areas within the cavernous sinus were misinterpreted as flow voids. The variable signal intensity of the cavernous sinus spaces on spin-echo MR images was probably due to different venous flow rates (15–17). Therefore, it might be difficult to differentiate normal venous flow in the cavernous sinus from abnormal flow voids in the presence of a CCF on spin-echo MR images.

It has been reported that enlargement of the SOV on the side of the CCF is seen in 86% to 100% and 75% to 100% of patients on contrast-enhanced CT scans and spin-echo MR images, respectively (1–5). In our study, enlargement of the SOV was found less frequently on the spin-echo MR images. Generally, with spin-echo imaging, the SOV is seen better on coronal sections (2, 3). Although the SOV was assessed mainly on coronal images in our study, the section selection may have affected the results of SOV evaluation on spin-echo images. The 3-D FISP images were relatively good at depicting enlarged

SOVs. The diameter of the SOV may change with head position or the Valsalva maneuver (18). The false-positive rate in our study was 1% to 4% among the three techniques; however, if enlargement of the SOV had been the only criterion for the diagnosis of CCF, a large number of false-positive findings would have been reported.

In our retrospective study, identification of the involved cavernous sinus with 3-D FISP images depended on the flow type of the CCF. Three CCFs that did not show hyperintensity in the cavernous sinus were of the slow type; therefore, there is a possibility of obtaining false-negative findings in patients with this type of CCF. Even when hyperintensity in the cavernous sinus is not seen on 3-D FISP images, one should carefully evaluate other findings related to venous drainage. In the fast type of dural CCF, we frequently observed multiple hyperintense curvilinear structures or spots adjacent to or within a cavernous sinus on 3-D FISP images in addition to the hyperintense areas within the sinus (Fig 3B). This finding may correspond to meningeal branches of the external and internal carotid arteries, representing the feeding pedicles of dural CCFs. Since this finding was not observed in direct CCFs, it may help to differentiate a direct CCF from a fast-type dural CCF on 3-D FISP images. Evaluation of posterior drainage, such as via the superior and inferior petrosal sinuses, was relatively difficult on CT scans and spin-echo MR images because these sinuses are relatively small and course adjacent to bone. The 3-D FISP images frequently showed the posterior drainage of CCFs because of their improved contrast resolution and flow-related enhancement. Transversely oriented 3-D FISP imaging may also be useful in the evaluation of the posterior drainage of CCFs. In our study, 3-D FISP images were not helpful for the evaluation of cortical venous drainage, probably as a result of saturation of drainage flow.

Contrast-enhanced 3-D time-of-flight MR angiography can be effective in examining venous structures and distal arteries (19, 20). However, in our study, the information referable to the flow dynamics within the cavernous sinuses was lost with the administration of contrast material because the cavernous sinuses enhanced homogeneously. Therefore, it was not possible to evaluate abnormal flow-related enhancement within the cavernous sinuses. Although draining vessels also enhanced, no additional information was obtained. Therefore, contrast administration is not needed in the evaluation of CCFs.

Our study has some limitations. First, although we excluded patients with mass lesions from the orbit to the cavernous sinus, and most were studied after treatment, many of the control subjects had diseases that may have affected the structures in the orbit and possibly the cavernous sinuses. Thus, whereas the lesions found in the control patients might have some effect on our blinded study, we believe that our study properly represents the clinical subjects. Second, in terms of the resolution of the 3-D FISP images, we used two different types of MR units. Most of the images were obtained with a 192×256 matrix; however, in three patients, high-resolution images were obtained with a 256×512 matrix. Although we did not evaluate the difference between these sequences, the 256×512 matrix offered better spatial resolution. Further study is needed to confirm whether high-resolution images improve the diagnosis of CCF. Newer MR imaging techniques, such as magnetization transfer contrast (21), may also improve the diagnostic accuracy of 3-D FISP imaging.

Conclusion

Three-dimensional FISP imaging was superior to spin-echo MR imaging and tended to be better than contrast-enhanced CT for the diagnosis of CCF. CT is substantially less costly, but has some disadvantages: it uses ionizing radiation, and its higher spatial resolution, which is obtained with the use of high matrices, thinner sections, and smaller fields of view, usually requires higher doses of radiation. Further, intravenous injection of a contrast agent is needed for the evaluation CCFs with CT. Therefore, we believe that unenhanced 3-D FISP imaging is a reliable method for the diagnosis of CCFs.

Acknowledgments

We are grateful to Charles E. Metz for providing the ROC-curve fitting program and to Ronald F. Budzik, Jr, for his valuable advice.

References

1. Ahmadi J, Teal JS, Segall HD, et al. **Computed tomography of carotid-cavernous fistula.** *AJNR Am J Neuroradiol* 1983;4:131–136
2. Hirabuki N, Miura T, Mitomo M, et al. **MR imaging of dural arteriovenous malformations with ocular signs.** *Neuroradiology* 1988;30:390–394
3. Komiyama M, Fu Y, Yagura H, et al. **MR imaging of dural AV fistulas at the cavernous sinus.** *J Comput Assist Tomogr* 1990;14:397–401
4. Elster AD, Chen MM, Richardson DN, Yeatts PR. **Dilated intercavernous sinuses: an MR sign of carotid-cavernous and carotid-dural fistulas.** *AJNR Am J Neuroradiol* 1991;12:641–645
5. Uchino A, Hasuo K, Matsumoto S, Masuda K. **MRI of dural carotid-cavernous fistulas: comparisons with postcontrast CT.** *Clin Imaging* 1992;16:263–268
6. Hirai T, Korogi Y, Sakamoto Y, et al. **MR angiography of the persistent trigeminal artery variant.** *J Comput Assist Tomogr* 1995;19:495–497
7. Du C, Korogi Y, Nagahiro S, et al. **Hemifacial spasm: three-dimensional MR images in the evaluation of neurovascular compression.** *Radiology* 1995;197:227–231
8. Korogi Y, Nagahiro S, Du C, et al. **Evaluation of vascular compression in trigeminal neuralgia by 3D time-of-flight MRA.** *J Comput Assist Tomogr* 1995;19:879–884
9. Tsuruda J, Saloner D, Norman D. **Artifacts associated with MR neuroangiography.** *AJNR Am J Neuroradiol* 1992;13:1411–1422
10. Chen J, Tsuruda JS, Halbach VV. **Suspected dural arteriovenous fistula: results with screening MR angiography in seven patients.** *Radiology* 1992;183:265–271
11. Swetz JA, Pickett RM. **Evaluation of Diagnostic Systems.** New York, NY: Academic Press; 1982
12. Hanley JA. **Receiver operating characteristic (ROC) methodology: the state of the art.** *Clin Rev Diagn Imaging* 1989;29:307–335
13. Metz CE. **ROC methodology in radiologic imaging.** *Invest Radiol* 1986;21:720–733

14. Metz CE. **Some practical issues of experimental design and data analysis in radiological ROC studies.** *Invest Radiol* 1989;24:234–245
15. Daniels DL, Pech P, Mark L, Pojunas K, Williams AL, Haughton VM. **Magnetic resonance imaging of the cavernous sinus.** *AJR Am J Roentgenol* 1985;144:1009–1014
16. Scotti G, Yu C, Dillon WP, et al. **MR imaging of cavernous sinus involvement by pituitary adenomas.** *AJNR Am J Neuroradiol* 1988; 9:657–664
17. Daniels DL, Czervionke LF, Bonneville JF, et al. **MR imaging of the cavernous sinus: value of spin echo and gradient recalled echo images.** *AJNR Am J Neuroradiol* 1988;9:947–952
18. Atlas SW, Galetta SL. **The orbit and visual system.** In: Atlas SW, ed. *Magnetic Resonance Imaging of the Brain and Spine.* 2nd ed. Philadelphia, Pa: Lippincott-Raven; 1996:1007–1092
19. Chakeres DW, Schmalbrock P, Brogan M, Yuanc C, Cohen L. **Normal venous anatomy of the brain: demonstration with gadopentetate dimeglumine in enhanced 3-D MR angiography.** *AJNR Am J Neuroradiol* 1990;11:1107–1118
20. Marchal G, Michiels J, Bosmans H, Hecke PV. **Contrast-enhanced MRA of the brain.** *J Comput Assist Tomogr* 1992;16: 25–29
21. Atkinson D, Brant-Zawadzki MN, Gillan GD, Purdy D, Laub G. **Improved MR angiography: magnetization transfer suppression with variable flip angle excitation and increased resolution.** *Radiology* 1994;190:890–894